

# Journal of Thermal Analysis and Calorimetry

## Kinetic of Pyrite thermal degradation under oxidative environment

--Manuscript Draft--

<b>Manuscript Number:</b>	JTAC-D-19-00517R2
<b>Full Title:</b>	Kinetic of Pyrite thermal degradation under oxidative environment
<b>Article Type:</b>	Research Paper
<b>Corresponding Author:</b>	Manuel Jesús Díaz Blanco, Ph.D. Universidad de Huelva UTRERA, Sevilla SPAIN
<b>Corresponding Author Secondary Information:</b>	
<b>Corresponding Author's Institution:</b>	Universidad de Huelva
<b>Corresponding Author's Secondary Institution:</b>	
<b>First Author:</b>	Marta Vázquez, Grade
<b>First Author Secondary Information:</b>	
<b>Order of Authors:</b>	Marta Vázquez, Grade
	Ignacio Moreno-Ventas, Dr.
	Irene Raposo, Grade
	Alberto Palma, Dr.
	Manuel Jesús Díaz Blanco, Ph.D.
<b>Order of Authors Secondary Information:</b>	
<b>Funding Information:</b>	
<b>Abstract:</b>	<p>Pyrite is the most common mineral in polymetallic sulphides ores. In order to apply the combustion group theory to the pyrometallurgical processes that occur in the reaction shaft it is necessary to know the kinetic processes that happen in pyrite. In this study a thermogravimetric analysis was carried out under oxidative atmospheric conditions with 100% O<sub>2</sub> and a heating ramp of 5, 10, 15 and 20 °C min<sup>-1</sup>. The material used was pyrite with a grain size of 63-125 µm. From the thermogravimetric data we got the kinetic parameters of the oxidative reactions of pyrite. The different kinetic methods used in this study have been E1641-16 ASTM, Ozawa-Flynn-Wall, Kissinger-Akahira-Sunose and Friedman.</p> <p>These methods were used for obtaining the kinetic parameters through Regression analysis, Sum of squares, mean residuals between experimental and calculated values and Student coefficient (95%) and to determine which kinetic method is the most suitable to describe the kinetics of pyrite oxidation.</p>
<b>Response to Reviewers:</b>	<p>Dear Dr. Alfréd Kállay-Menyhárd</p> <p>According to your letter, the modifications have been not highlighted in the previous revised version.</p> <p>In this version, the modifications (with except to the acronyms) have been highlighted in the text.</p> <p>Regards</p>

## Kinetic of Pyrite thermal degradation under oxidative environment

Vázquez, M.<sup>1</sup>, Moreno-Ventas, I.<sup>1</sup>, Raposo, I.<sup>1</sup>, Palma, A.<sup>2</sup>, Díaz, M.J.<sup>2</sup>

<sup>1</sup>Facultad de Ciencias Experimentales, University of Huelva, Huelva, 21007, Spain. Centro de Investigación en Química Sostenible (CIQSO), University of Huelva, Huelva, 21007, Spain

<sup>2</sup>Escuela Técnica Superior de Ingeniería, University of Huelva, Huelva, 21007, Spain. Centre for Research in Product Technology and Chemical Processes (Pro2TecS), University of Huelva, Huelva, 21007, Spain

Moreno-Ventas, I. (<https://orcid.org/0000-0002-7927-5212>), Palma, A. (<https://orcid.org/0000-0003-0420-1785>), Díaz, M.J. (<https://orcid.org/0000-0002-5059-4340>)

### Abstract:

Pyrite is the most common mineral in polymetallic sulphides ores. In order to apply the combustion group theory to the pyrometallurgical processes that occur in the reaction shaft it is necessary to know the kinetic processes that happen in pyrite. In this study a thermogravimetric analysis was carried out under oxidative atmospheric conditions with 100% O<sub>2</sub> and a heating ramp of 5, 10, 15 and 20 °C min<sup>-1</sup>. The material used was pyrite with a grain size of 63-125 µm. From the thermogravimetric data we got the kinetic parameters of the oxidative reactions of pyrite. The different kinetic methods used in this study have been E1641-16 ASTM, Ozawa-Flynn-Wall, Kissinger-Akahira-Sunose and Friedman. These methods were used for obtaining the kinetic parameters through Regression analysis, Sum of squares, mean residuals between experimental and calculated values and Student coefficient (95%) and to determine which kinetic method is the most suitable to describe the kinetics of pyrite oxidation.

**Keywords:** Pyrite, Thermogravimetry, Sulphide, Kinetic, Ozawa-Flynn-Wall, Kissinger-Akahira-sunose, Friedman, ASTM-E1641.

## 29 1. Introduction

30 Pyrite ( $\text{FeS}_2$ ) is the most common mineral in sulphide ores. It is composed of 53.48% sulphur and 46.52%  
31 iron [1] and it has cubic structure with unit-cell edge around  $5.42\text{\AA}$ . Usually appears in association with  
32 other minerals such as chalcopyrite ( $\text{CuFeS}_2$ ), galena ( $\text{PbS}$ ), tetradrite ( $\text{Cu}_6[\text{Cu}_4(\text{Fe,Zn})_2]\text{Sb}_4\text{S}_{13}$ ),  
33 chalcocite ( $\text{Cu}_2\text{S}$ ) and sphalerite ( $\text{ZnS}$ ) [2].

34 To use polymetallic sulphides in extractive copper pyrometallurgical processes it is necessary to enrich  
35 sulphide ores in copper through grinding and flotation techniques to increase copper concentration from  
36 0.5-2 Wt. % to a material called "concentrate" (Fig.1) with a copper concentration of 20-30 Wt. % [3, 4].

37  
38 **Fig. 1: BSE (Back-scattered Electron) image of a concentrate obtained through an electronic**  
39 **microprobe model JEOL, model JXA-8200 Super probe. Working conditions used were an**  
40 **acceleration voltage of 15 kV and a current of 20 nA of beam intensity with an electron beam**  
41 **diameter between 1 and 5  $\mu\text{m}$ . Py: Pyrite ( $\text{FeS}_2$ ), Dg: Digenite ( $\text{Cu}_9\text{S}_5$ ), Mb: Molybdenite ( $\text{MoS}_2$ ).**

42 The concentrates are blended to get a regular composition material to minimise the fluctuation of the  
43 pyrometallurgy process.

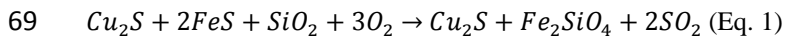
44 Oxidative melting of the blend is made through two stages (Flash smelting and conversion processes) in  
45 order to minimise copper losses. [3].

46 In the first stage, two immiscible liquids are produced through flash smelting: matte and slag [5]. Matte is  
47 a melt composed of  $\text{FeS}$  and  $\text{Cu}_2\text{S}$  (usually the matte grade is around 62 wt.% Cu). Slag melts are  
48 composed, mainly, of fayalite ( $\text{Fe}_2\text{SiO}_4$ ) and magnetite ( $\text{Fe}_3\text{O}_4$ ) in a proportion that depends on oxygen  
49 partial pressure (usually  $10^{-7}$  atm for flash smelting). The liquid immiscibility region between slag and  
50 matte was shown by the experimental work of Yazawa and Kameda [6] over the ternary system of  $\text{SiO}_2$ -  
51  $\text{FeO}$ - $\text{FeS}$  (Fig. 2).

52  
53 **Fig. 2: Isothermal phase diagram ( $\text{FeO}$ - $\text{FeS}$ - $\text{SiO}_2$ ) based on Yazawa and Kameda [6]. Point A and B**  
54 **are in equilibrium and marks, respectively, the composition of an oxide rich melt (slag) and the**  
55 **composition of a sulphide rich melt (matte). Both compositions, A and B correspond to the**  
56 **equilibrium compositions of slag and matte at the limit of silica solubility. To the right of line A-B**  
57 **the immiscible melts coexist with solid silica.**

59 As it is showed in the isothermal phase diagram for the system FeO-FeS-SiO<sub>2</sub> [6], the blends are brought  
60 inside the immiscibility region by addition of SiO<sub>2</sub> (arrow in bold in Figure 2) as a flux component for  
61 melting. The objective to take the system inside the liquid immiscibility region is to get two immiscible  
62 liquids (slag and matte) in order to extract part of the iron in concentrates to the slag and the copper to the  
63 matte. In this process it is very important to minimize the copper dissolution in the slag melts through a  
64 control of the oxygen partial pressure.

65 After the first stage, in the conversion process the matte melts are transformed in blister copper through  
66 two oxygen-blowing stages. In the first stage (slag blowing) the oxygen reacts with FeS to produce iron  
67 and sulphur dioxide. At the same time, iron reacts with the silica flux to make fayalite (Fe<sub>2</sub>SiO<sub>4</sub>). This  
68 blowing stage produces white metal melt (Cu<sub>2</sub>S) (Eq.1):

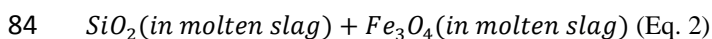
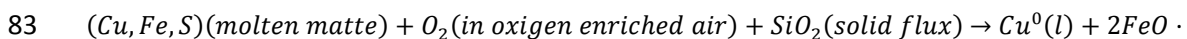


71 The white metal produced in slag blowing is used to get copper blister through the second stage of  
72 oxidation named Copper blowing [7] (Fig. 3).

74 **Fig. 3: Equilibrium phase diagram from Sharma and Chang [7]. The dotted line marks the**  
75 **different compositions (Points a, b, c and d) of the conversions process at 1200 °C in copper**  
76 **blowing.**

78 The equilibrium phase diagram (Fig. 3) shows the copper blowing stage at 1200 °C. Beginning with the  
79 white metal (Point a) the system goes into a new liquid immiscible region to give molten blister copper  
80 plus molten white metal. As the oxidative process goes on the proportion of blister copper increase from  
81 point b to point c generating an SO<sub>2</sub> gas phase.

82 Schematically, the conversion process follows the next reaction (Eq. 2):



85 Oxidative melting of blends, of sulphides concentrates, in the flash-smelting step depends on process  
86 parameters as ignition temperature and combustion kinetic of the sulphides. Both parameters are relevant  
87 for the process in the reaction flame produced at the end of the burner located at the top of the reaction

1  
2  
3  
4  
5  
6  
7  
8  
9  
10  
11  
12  
13  
14  
15  
16  
17  
18  
19  
20  
21  
22  
23  
24  
25  
26  
27  
28  
29  
30  
31  
32  
33  
34  
35  
36  
37  
38  
39  
40  
41  
42  
43  
44  
45  
46  
47  
48  
49  
50  
51  
52  
53  
54  
55  
56  
57  
58  
59  
60  
61  
62  
63  
64  
65

88 shaft within the flash furnace. As the flame oxidative melting is a time limited process, the combustion  
89 kinetic of each type of sulphides is relevant for the global process.

90 Ignition of sulphides concentrates (blends) is an exothermic process that starts for the most reactive  
91 sulphide grains and spread to the rest of grains through radiative heat flow. The application of the group  
92 combustion theory to the flash smelting process data about the kinetics of sulphides species are required.

93 Most of the studies carried out about sulphides oxidative evolution focus on the analysis of mechanisms  
94 of oxidation processes, thermogravimetric behaviour of minerals versus variations in mineral grain sizes  
95 and intrinsic water content or differences in the composition of the working gas [8-13].

96 To analyse in deep the oxidative-melting in pyrometallurgical process taken over metallurgical copper  
97 sulphide concentrates (blends) it is necessary to understand the oxidation kinetics of each type of the  
98 sulphides that composes the concentrates used in the industrial copper extractive metallurgy. Pyrite is a  
99 sulphide usual in concentrates and has an important role in the process temperature of the copper flash  
100 smelting. Then it is relevant to study and determine the combustion kinetic of pyrite.

101 In this study the reaction kinetic evolution of the pyrite oxidation process by studying different kinetics  
102 methods is analysed to determine the suitable kinetic method for use with pyrite, from thermogravimetry  
103 studies performed on pyrite minerals. The kinetics methods used are E1641-16 [14], Ozawa/Flynn/Wall  
104 [15-17], Kissinger-Akahira-Sunose (KAS) [18, 19] and Friedman [20].

## 106 2. Materials and Methods

### 107 2.1. Raw materials

108 The composition of the pyrite is usually pure although in some occasions there may be substitutions of  
109 metallic elements such as Ni, Co or more rarely Cu replacing the Fe.

110 The pyrites are quite chemically stable, we checked it by studying 40 different pyrite compositions  
111 obtained through the RRUFF database [1]. This similarity of compositions gives us that the  
112 thermogravimetry study is significant and it has a wide validity because there are no variations in the  
113 composition.

114 The average composition of the pyrites, according to the Rruff database is 46.76% Fe and 53.24% S.

115 The pyrite was crushed and screened into the fraction 63-125  $\mu\text{m}$  for used in the study.

116 The pyrite sample used for the study was analyzed by x-ray diffraction model BRUKER D8 Advance, in  
117 Bragg-Brentano geometry, using copper  $K\alpha$  radiation ( $K\alpha = 1,5406 \text{ \AA}$ ) excited by a current of 30 mA of

118 intensity and 40 kV of voltage. The working conditions were a scan interval of 3 to 65 ° of 2  $\theta$ , an  
119 increase of angle step of 0.2 ° of 2  $\theta$ , and an exposure time per step of 0.6s.

120 The treatment and evaluation of diffractometry data is done using the DIFFRACplus software and  
121 X Powder.12 software used with the database AMSCD (American Mineralogist Crystal Structure  
122 Database).

123 The diffractogram obtained shows that the sample used during the study was of pyrite composition. (Fig.  
124 4).

125

126 **Fig. 4: Pyrite diffractogram pointing to the D-Spacing in amperes.**

127

## 128 **2.2. TG experiments**

129 A thermo-gravimetric analyzer (TG) (Mettler Toledo TG/DSC1 STARe System) has been used to study  
130 pyrite thermo-chemical oxidation behavior. The experiments were performed by heating 70-130 mg  
131 sample under a temperature range of 25-900°C and four heating rates of 5, 10, 15 and 20°C min<sup>-1</sup> and 20  
132 cm<sup>3</sup> min<sup>-1</sup> oxygen flow has been also used. Pyrite oxidation kinetic data, based on Arrhenius activation  
133 energy ( $E_a$ ) and pre-exponential constant ( $A$ ) from TG data have been calculated by using four proven  
134 free isoconversional methods such as: E1641-16 [14], Ozawa/Flynn/Wall [15-17], Kissinger-Akahira-  
135 Sunose (KAS) [18, 19] and Friedman [20] models. In this form, the reactions processes could be studied  
136 without the assumption of any kinetic model. NETZSCH Kinetics Neo® software to analyze thermo-  
137 chemical processes data has been used. Among above mentioned studied methods, the most suitable  
138 statistical data obtained have been exposed.

139

## 140 **3. Results and Discussion**

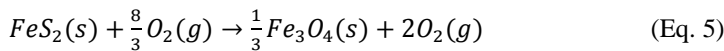
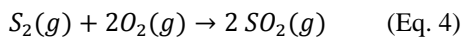
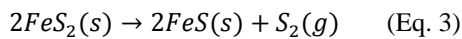
### 141 **3.1. Thermogravimetric analysis of the thermochemical process.**

142 The TG and DTG (first derivative TG curve) for pyrite (mean of the three replicates per heating rate) over  
143 the range of temperature from 25 °C to 850 °C under four heating rates (5, 10, 15 and 20 °C min<sup>-1</sup>) and  
144 oxygen atmosphere are shown in Figures 5 and 6 respectively. The Fig 5 and 6 show that different results,  
145 for each studied heating rate, are obtained. Main differences in the obtained curve at 5 °C/min have been  
146 observed. In general, TG curves show that the oxidation reactions for pyrite in a range from 440-500 °C  
147 and from 500-850 °C approximately have been observed. Specifically, an initial pyrite degradation at 440

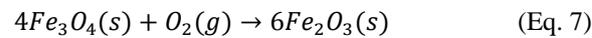
148 °C (Fig. 6), with a loss of mass (approximately 30% of the initial mass) have been observed in Fig. 5.  
 149 According to Zivkovic et al. [21] the first degradation could be due to a pyrite dissociation following Eq.  
 150 3. In this sense, it is worth mentioning that in the study carried out by Zivkovic et al., [21] the first loss of  
 151 mass occurred at 370 °C, at 350 °C for Zhou [22]. Earnest [23] described the degradation at 400 °C. The  
 152 oxidation of Pyrite for Hongfei Chen [24] starts at 400 °C, Pérez et al., [13] among 485 to 625 °C, Dunn  
 153 et al., [25] among 425-435 °C, Dunn [26] among 330 to 630 °C and for Zhou [22] the main mass loss  
 154 occurred at 450 °C. The obtained sulphur, under an oxidative atmosphere, had been oxidized to SO<sub>2</sub> (Eq.  
 155 4) and the oxidation of FeS<sub>2</sub> to magnetite (Fe<sub>3</sub>O<sub>4</sub>, Eq.5) could also have taken place at that temperature.

157 **Fig. 5: Thermal gravimetric analysis of pyrite with 100% O<sub>2</sub>.**

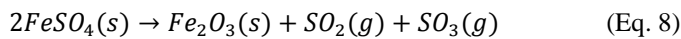
159 **Fig. 6: Differential thermal gravimetric analysis of pyrite with 100% O<sub>2</sub>.**



164  
 165 After the first degradation phase, under an increase in temperature ( $\approx 480$  °C), occurred a sulphation (Eq. 6  
 166 and magnetite was oxidized to hematite (Eq. 7), which leads to a slight increase (0.3% of the initial mass)  
 167 in mass (Fig 6),



170 Under high temperatures ( $\geq 650$  °C) the formed iron (II) sulphate was degraded (approximately 3.5% of  
 171 the initial mass) into hematite (iron (III) oxide, Eq. 8)



174 **3.2. Analysis of pyrite oxidation kinetics**

175 The kinetic parameters were calculated by using the above mentioned model-free methods. As expected,  
 176 not all studied models are in agreement to an adequate fit for the oxidative degradation of pyrite. Thus, in

177 Table 1 the main statistical values (regression analysis, sum of deviation squares, mean residuals between  
178 experimental and calculated values and Student coefficient) calculated from the models are shown.

179 From Table 1, among the studied methods, Kissinger's method seems to be the best way to describe the  
180 oxidative thermal behavior of pyrite.

181 The KAS method [19] (Eq. 9) is an extension to the 0.1-0.9 interval of the initial Kissinger model [18]. In  
182 this sense, KAS's kinetic method is an isoconversional method where the activation energy is a function  
183 of the conversion degree of a chemical reaction and can be applied without any assumption concerning  
184 the kinetic model  $f(\alpha)$ .

$$185 \quad \ln\left(\frac{\beta_i}{T_{jk}^2}\right) = \ln\left(\frac{A_{0\alpha}R}{E_{a\alpha}}\right) - \frac{E_{a\alpha}}{RT_{jk}} - \ln g(\alpha_k) \quad \text{Eq. 9}$$

186 where  $E_{a\alpha}$  and  $A_{0\alpha}$  are the apparent activation energy and the pre-exponential factor at a given conversion  
187 degree  $\alpha_k$ , and the temperatures  $T_{jk}$  are those which the conversion  $\alpha_k$  is reached at a heating rate  $\beta_j$  for a  
188 series of experiments at different heating rates ( $\beta$ ). In this form,  $T_{jk}$  is the temperature peak of the DTG  
189 curve and a series of different heating rate measurements are ( $\beta_{l,j}$ ) required in this model (Fig. 7).

191 **Fig. 7: Kissinger-Akahira-Sunose plot of pyrite.**

192  
193 The apparent activation energy and Arrhenius pre-exponential factor (under different conversion grade)  
194 could be obtained from the slope and the intercept, respectively, of the linear plot of  $\ln\left(\frac{\beta_i}{T_{jk}^2}\right)$  vs.  $1/T_{jk}$ .

195 According to Eq. 9 several conversion ( $\alpha$ ) values (0.1 to 0.9) for all curves (different heating rates) have  
196 been evaluated. The KAS equation (slope and  $R^2$ ) shows a high relationship between of  $\ln(\beta/T_{jk}^2)$  and  
197  $1000/T_{jk}$  (Fig. 7). Therefore, this method for obtaining the activation energy for thermochemical oxidation  
198 of pyrite is considered suitable. After that, apparent activation energy ( $E_a$ ) values could be assessed from  
199 the slopes of these equations for each  $\alpha$ . As shown in Figure 7, the obtained slopes, and therefore, the  
200 calculated values for apparent  $E_a$ , regardless of the rate of heating, appear to be similar. The  $\alpha$  values  
201 from 0.1 to 0.9 on the curve obtained at  $15 \text{ }^\circ\text{C min}^{-1}$  (medium value) heating rate have been chosen to  
202 determine the kinetic parameters. In Figure 8, the calculated  $E_a$  values results show that the activation  
203 energy was not similar for all conversion indicates the existence of a complex mechanism that occurs in  
204 the solid state.

205

206 **Fig. 8: Apparent activation energy ( $E_a$ ) values for pyrite thermal oxidative degradation calculated**  
207 **from the KAS equation for each conversion grade ( $\alpha$ ) value.**

208

209 In Figure 9 an evolution of the pre-exponential factor ( $A$ ) is shown. It is important to note that, according  
210 to Vyazovkin [27], model-free kinetic models have the inconvenience of treating the experimental value of  
211  $A$  as a dependent parameter. **In spite of this**, similar behavior to that described for  $E_a$ , can be observed for  
212 this parameter.

213

214 **Fig. 9: Fig. 12: Pre-exponential factor ( $A$ ) values calculated from the KAS equation for each**  
215 **conversion grade ( $\alpha$ ) value.**

216

217 The obtained  $E_a$  and  $A$  values were highly dependent on the extent of conversion which could indicate  
218 that the process must be described as a multi-step reaction. The calculated  $E_a$  values at the different  
219 conversion rates show higher values under low conversion degree (200-450 kJ mol<sup>-1</sup>). The initial increase  
220 in activation energy conversion may be attributed to ignition and pyrite oxidation (Eq. 3-5). After that, a  
221 progressive decline to values close to 80 kJ mol<sup>-1</sup> at  $\alpha=0.8$  is found. The lower kinetic values of  $E_a$  and  $A$   
222 values obtained under high conversion values, compared to those obtained in the initial reaction zone,  
223 may be due to the fact that magnetite which had lower decomposition rate than hematite. There may also  
224 have been a catalytic effect from inorganic elements on that degradation.

225

#### 226 **4. Conclusions**

227 Thermal degradation kinetic for oxidation process of pyrite have been studied in TG by using E1641-16,  
228 Ozawa/Flynn/Wall, Kissinger-Akahira-Sunose and Friedman models.

229 The most suitable model, among those studied, seems to be the one proposed by Kissinger.

230 The oxidation process of pyrite can be described as a multi-step reaction because values of  $E_a$  and  $A$  were  
231 highly dependent on the degree of conversion.

232 The calculated  $E_a$  values ranged among 450 kJ mol<sup>-1</sup> at  $\alpha=0.3$  and 80 kJ mol<sup>-1</sup> at  $\alpha=0.8$ .

233

#### 234 **5. References**

- 1  
2  
3  
4  
5  
6  
7  
8  
9  
10  
11  
12  
13  
14  
15  
16  
17  
18  
19  
20  
21  
22  
23  
24  
25  
26  
27  
28  
29  
30  
31  
32  
33  
34  
35  
36  
37  
38  
39  
40  
41  
42  
43  
44  
45  
46  
47  
48  
49  
50  
51  
52  
53  
54  
55  
56  
57  
58  
59  
60  
61  
62  
63  
64  
65
- 235 [1] RRUFF™ Project database <http://rruff.info/pyrite/display=default/> (accessed 13 March 2019)
- 236 [2] Zussman J, Howie RA, Deer WA. An introduction to the rock forming minerals. An Introduction to  
237 the Rock-Forming Minerals, 2nd edition. London (Longman Scientific and Technical). 1992.  
238 <https://doi.org/10.1180/minmag.1992.056.385.20>.
- 239 [3] Schlesinger ME, King MJ, Sole KC, Davenport WG. Extractive Metallurgy of Copper. Elsevier  
240 Science. London. 2011.
- 241 [4] Sancho JP, Verdeja LF, Ballester A. Metalurgia Extractiva. Volumen II: Procesos de obtención,  
242 Edited by Sintesis, Madrid, Spain, ISBN 84-7738-803-2. 2000.
- 243 [5] Davenport WG, Jones DM, King MJ, Partelpeog EH. Flash Smelting: Analysis, Control and  
244 Optimization. 2th Ed. T The Minerals, Metals and Materials Society (TMS). Pittsburgh, PA. 2003.
- 245 [6] Yazawa A, Kameda A, Copper Smelting. I. Partial liquidus diagram for FeSFeO-SiO<sub>2</sub> system. Tech  
246 Rep Tohoku Univ. 1953;16: 40-58.
- 247 [7] Sharma RC, Chang YA. A thermodynamic analysis of the copper sulfur system. Metall Transac B.  
248 1980; 11B: 575-583.
- 249 [8] Dunn JG, Jayaweera SAA. Applications of thermoanalytical methods to studies of flash smelting  
250 reactions. Thermochim Acta. 1985. [https://doi.org/10.1016/0040-6031\(85\)85543-X](https://doi.org/10.1016/0040-6031(85)85543-X)
- 251 [9] Dunn JG, De GC, O'Connor BH. The effect of experimental variables on the mechanism of the  
252 oxidation of pyrite: Part 1. Oxidation of particles less than 45 µm in size. Thermochim Acta. 1989;  
253 145: 115-130.
- 254 [10] Reimers GW, Hjelmstad KE. Analysis of the oxidation of chalcopyrite, chalcocite, galena,  
255 pyrrhotite, marcasite and arsenopyrite. Dept. of the Interior, Bureau of Mines. Report of  
256 investigations (United States. Bureau of Mines): 1987; 9118. Pittsburgh, Pa. U.S.
- 257 [11] Jorgensen FRA, Moyle FJ, Wadsley MW. Structural changes associated with the ignition of pyrite  
258 and chalcopyrite during flash smelting. In: Process Mineralogy IX, International symposium of  
259 Applied Mineralogy MAC-ICAM-CAN. 1989; 14-17 May. Montreal. CA. 323-341,
- 260 [12] Perez-Tello M, Sohn HY, Löttiger J. Determination of the oxidation characteristics of solid copper  
261 matte particles by differential scanning calorimetry and thermogravimetric analysis. Mining Metall  
262 Explorat. 1999. <https://doi.org/10.1007/BF03402800>.

- 263 [13] Pérez-Fontes SE, Pérez-Tello M, Prieto-López LO, Brown F, Castellón-Barraza F. Thermoanalytical  
264 study on the oxidation of sulfide minerals at high temperatures. *Min Metal Process.* 2007.  
265 <https://doi.org/10.1007/bf03403377>.
- 266 [14] ASTM Test Method E1641. Standard Test Method for Decomposition Kinetics by  
267 Thermogravimetry, ASTM Book of Standards 14.02, American Society for Testing and Materials,  
268 pp. 1042-1046. 1994.
- 269 [15] Ozawa T. A new method of analyzing thermogravimetric data, *Bull Chem Soc Jap.* 1965.  
270 <https://doi.org/10.1246/bcsj.38.1881>.
- 271 [16] Ozawa T (1965) Kinetic analysis of derivative curves in thermal analysis. *J Thermal Anal Calorim* 2  
272 (3): 301-324. <https://doi.org/10.1007/BF01911411>.
- 273 [17] Flynn J, Wall L. A quick, direct method for the determination of activation energy from  
274 thermogravimetric data. *Journal of Polymer Science Part B: Polym Let.* 1966; 4 (5): 323-328.
- 275 [18] Kissinger HE. Variation of peak temperature with heating rate in differential thermal analysis. *J Res*  
276 *Nat Bur Stand.* 1956. <https://doi.org/10.6028/jres.057.026>.
- 277 [19] Akahira T, Sunose T. Method of determining activation deterioration constant of electrical insulating  
278 materials. *Res Report Chiba Inst Technol (Sci Technol).* 1971; 16: 22-31.
- 279 [20] Friedman HL. Kinetics of thermal degradation of char-forming plastics from thermogravimetry.  
280 Application to a phenolic plastic. *J Polym Sci Part C.* 1964; 6: 183-195.
- 281 [21] Živković ŽD, Mitevska N, Savović V. Kinetics and mechanism of the pyrite-pyrite concentrate  
282 oxidation process. *Thermochim Acta.* 1996. [https://doi.org/10.1016/0040-6031\(96\)02883-3](https://doi.org/10.1016/0040-6031(96)02883-3).
- 283 [22] Zhou, Y., Xu, P., Cheng, H., & Liu, Q. (2018). Thermal phase transition of pyrite from coal. *Journal*  
284 *of Thermal Analysis and Calorimetry*, 134(3), 2391-2396.
- 285 [23] Earnest CM. Descriptive oxidative profiles for pyrite in the low temperature ash component of coals  
286 by differential thermal analysis. *Thermochim Acta.* 1984; 75(1-2): 219-232.
- 287 [24] Cheng, H., Liu, Q., Huang, M., Zhang, S., & Frost, R. L. (2013). Application of TG-FTIR to study  
288 SO<sub>2</sub> evolved during the thermal decomposition of coal-derived pyrite. *Thermochimica acta*, 555,  
289 1-6.
- 290 [25] Dunn JG, De GC, O'Connor BH. The effect of experimental variables on the mechanism of the  
291 oxidation of pyrite: Part 2. Oxidation of particles of size 90–125 μm. *Thermochim Acta.* 1989;  
292 155: 135-149.

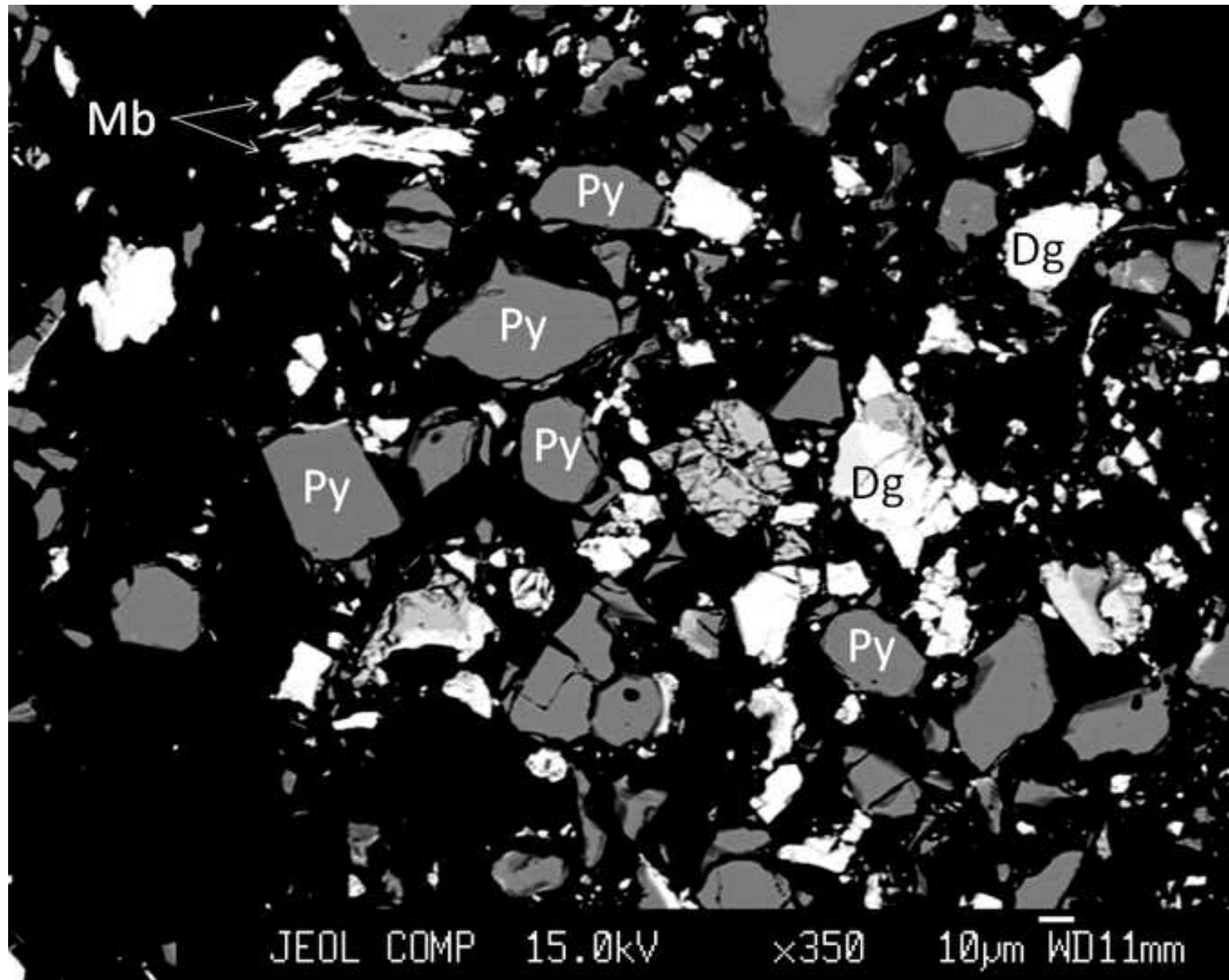
1  
2  
3  
4  
5  
6  
7  
8  
9  
10  
11  
12  
13  
14  
15  
16  
17  
18  
19  
20  
21  
22  
23  
24  
25  
26  
27  
28  
29  
30  
31  
32  
33  
34  
35  
36  
37  
38  
39  
40  
41  
42  
43  
44  
45  
46  
47  
48  
49  
50  
51  
52  
53  
54  
55  
56  
57  
58  
59  
60  
61  
62  
63  
64  
65

293 [26] Dunn JG. The oxidation of sulphide minerals. *Thermochim Acta* . 1997; 300 (1-2): 127-139.

294 [27] Vyazovkin S. Model-free kinetics. Staying free of multiplying entities without necessity. *J Therm*

295 *Anal Calorim.* 2006. <https://doi.org/10.1007/s10973-005-7044-6>.

Figure 1



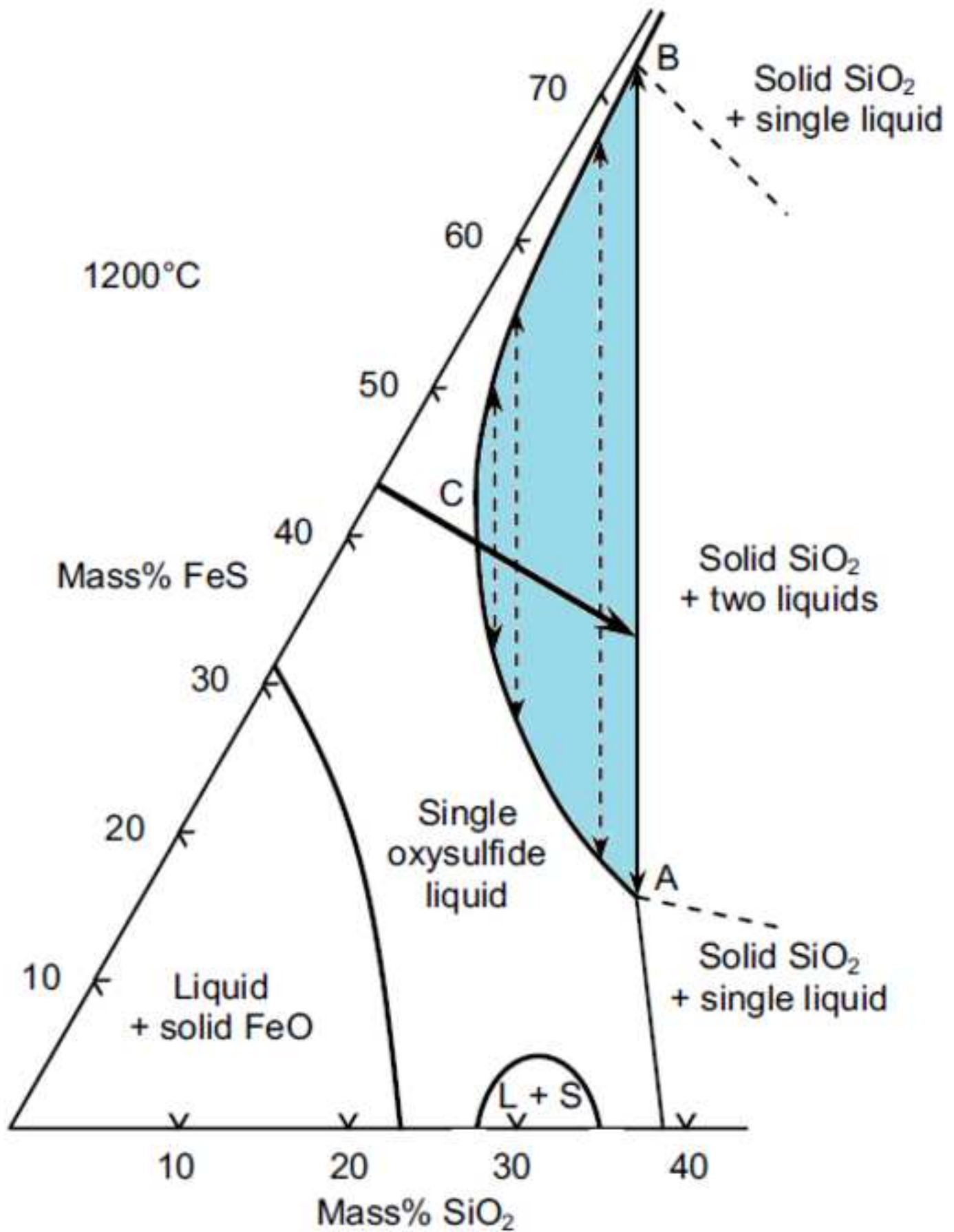


Figure 3

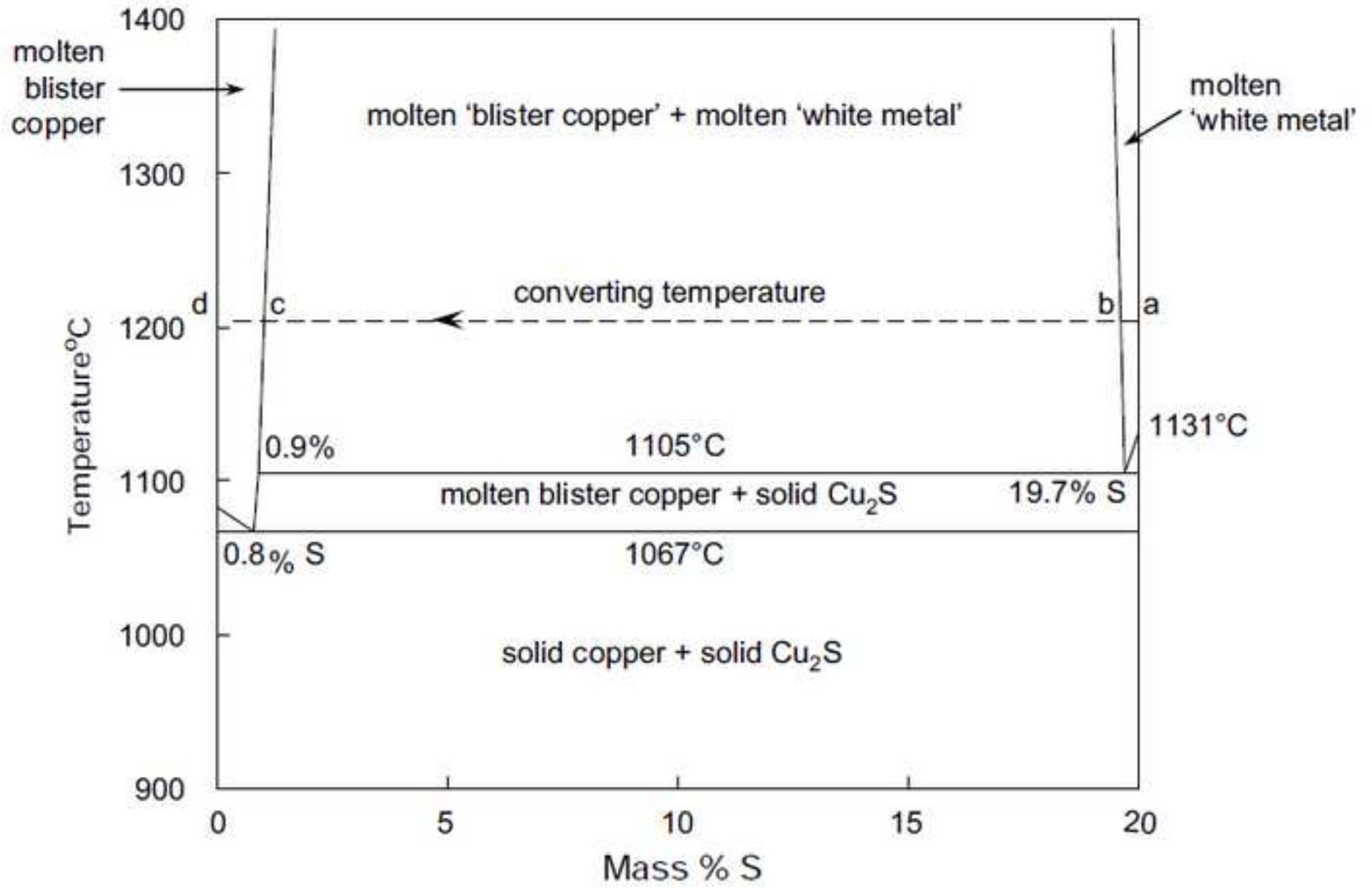
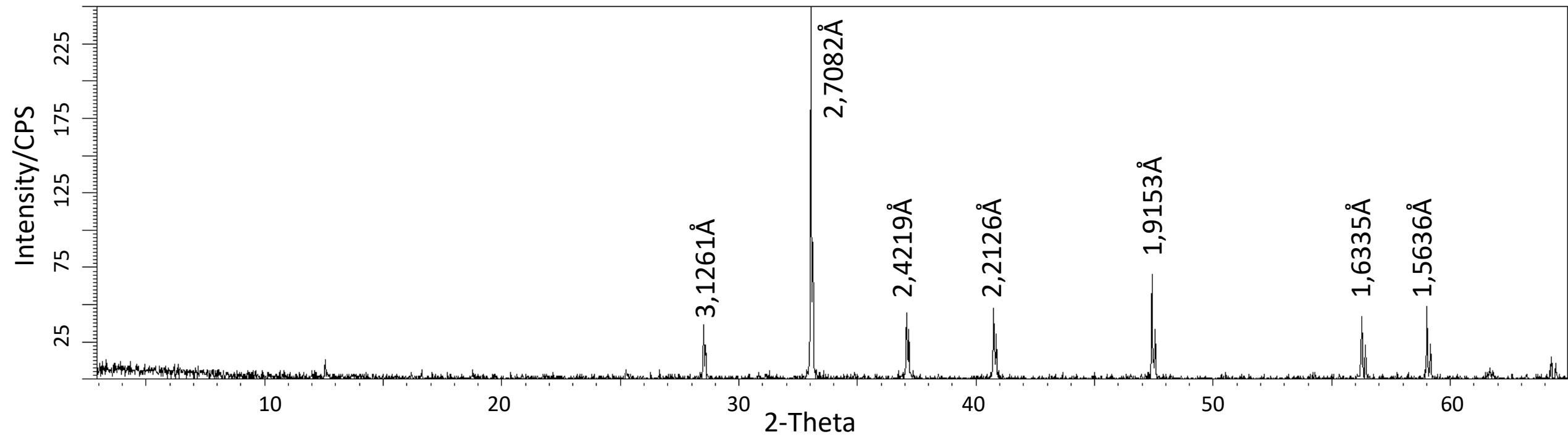
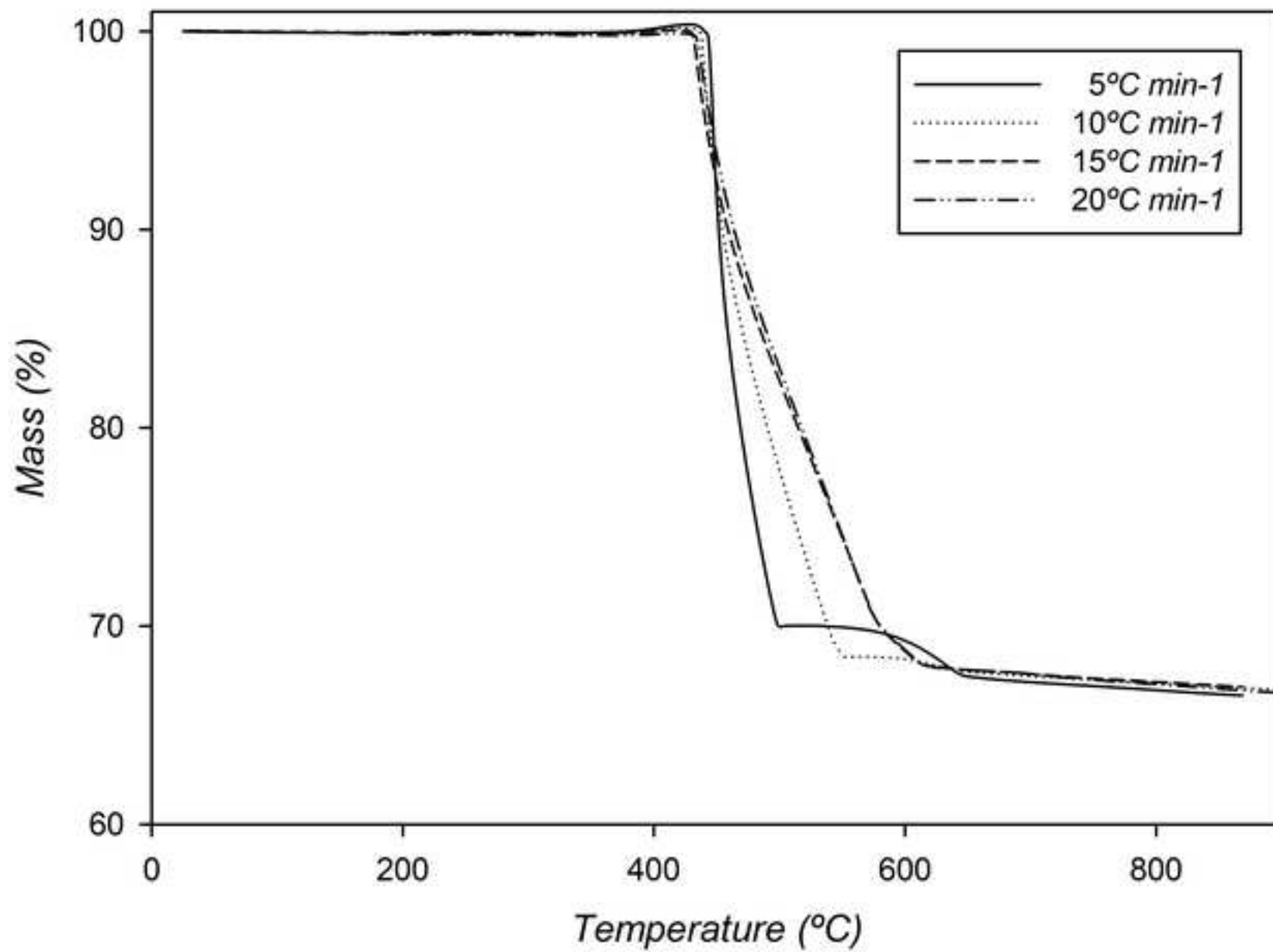


Figure 4





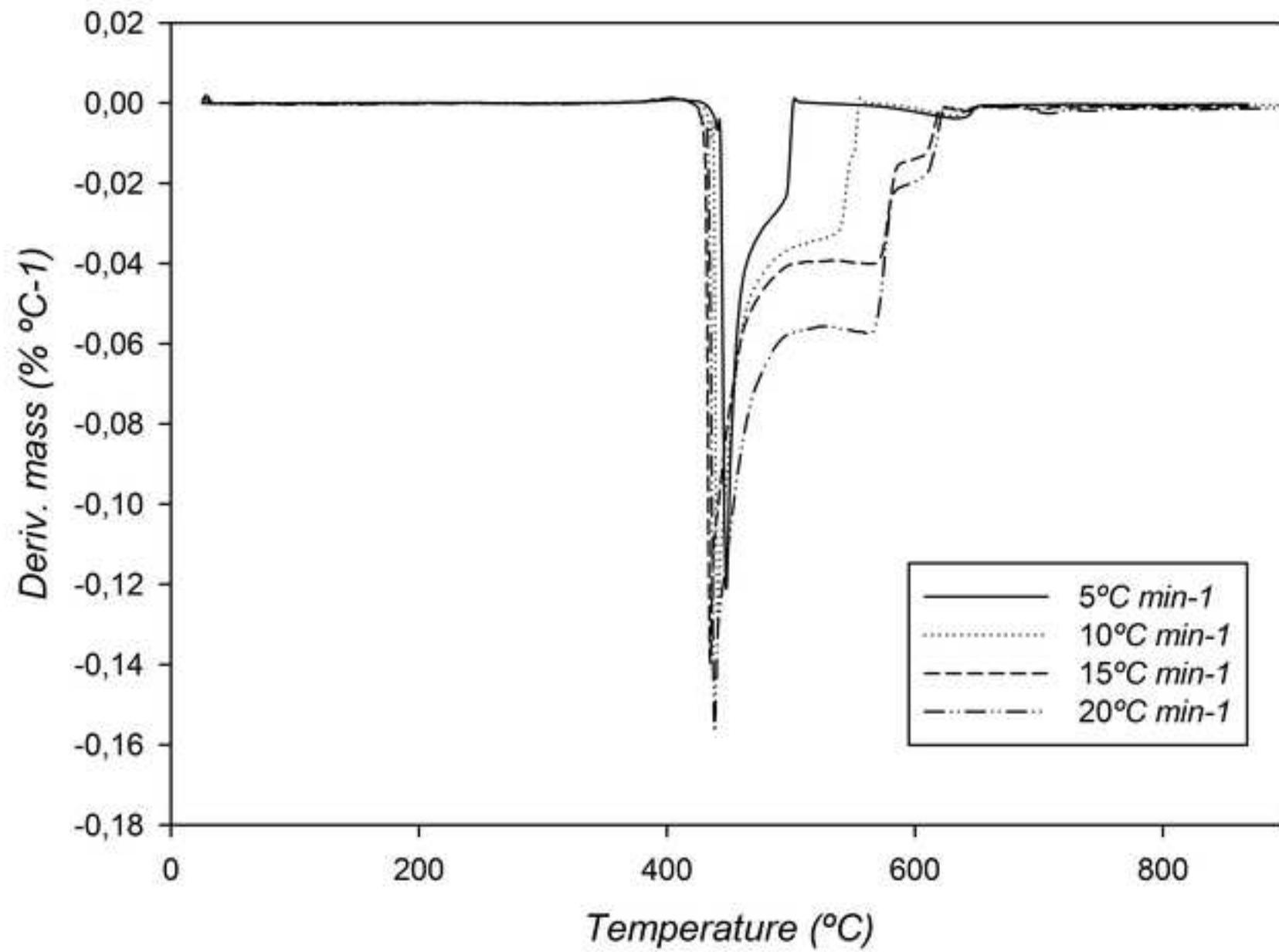
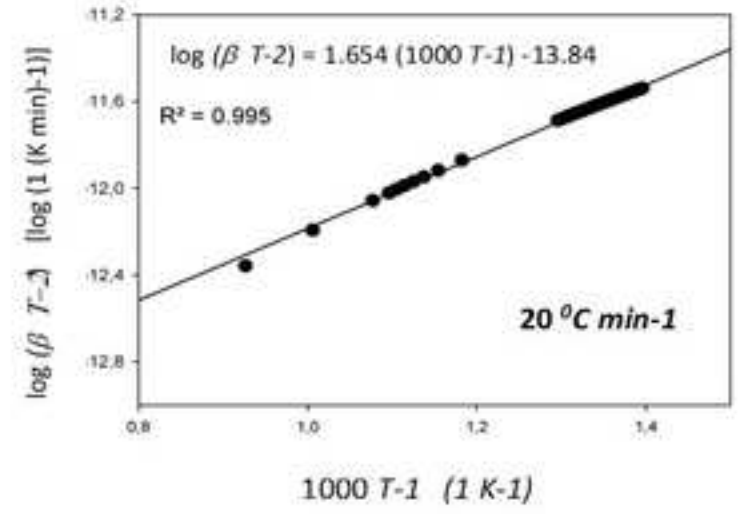
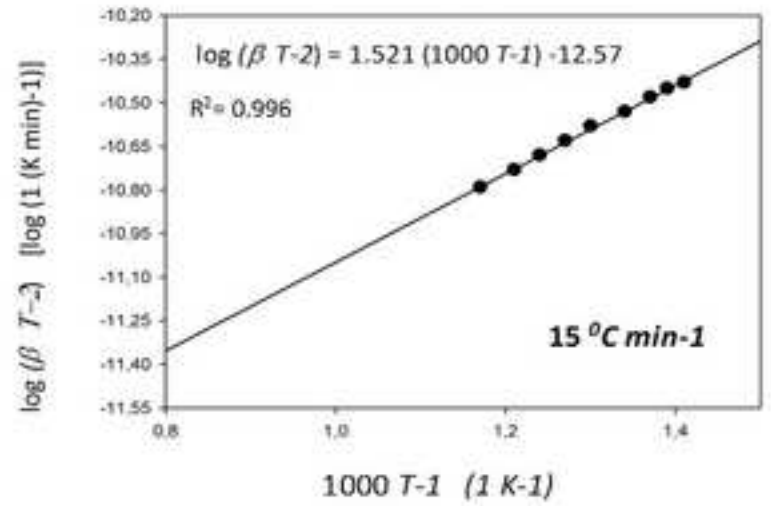
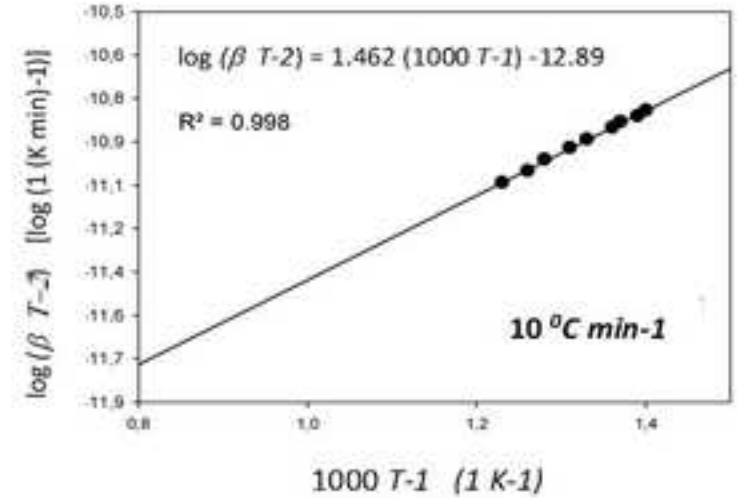
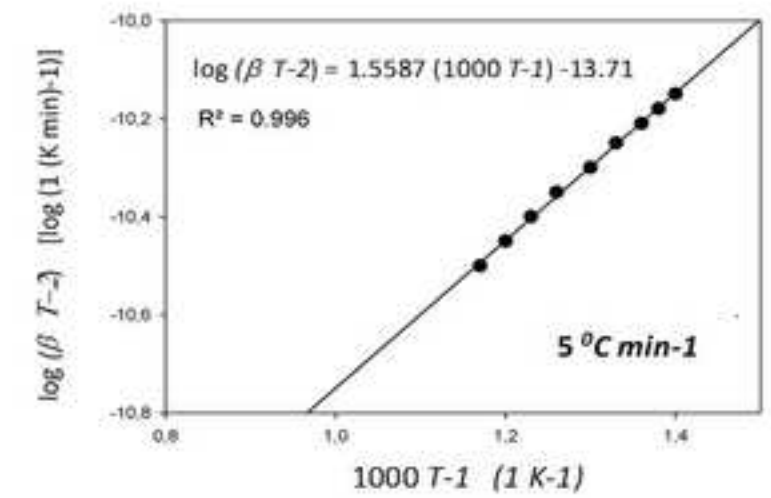
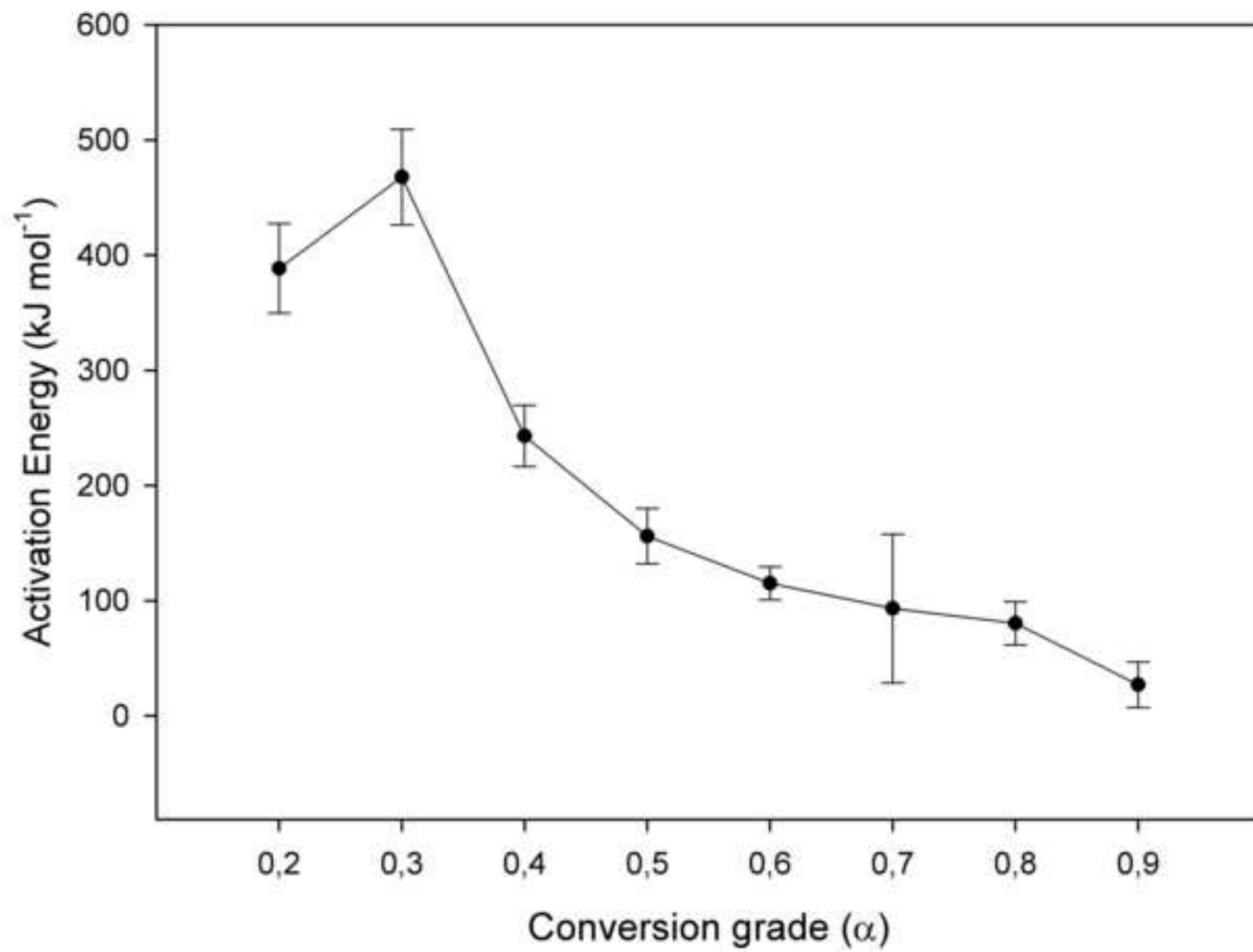


Figure 7





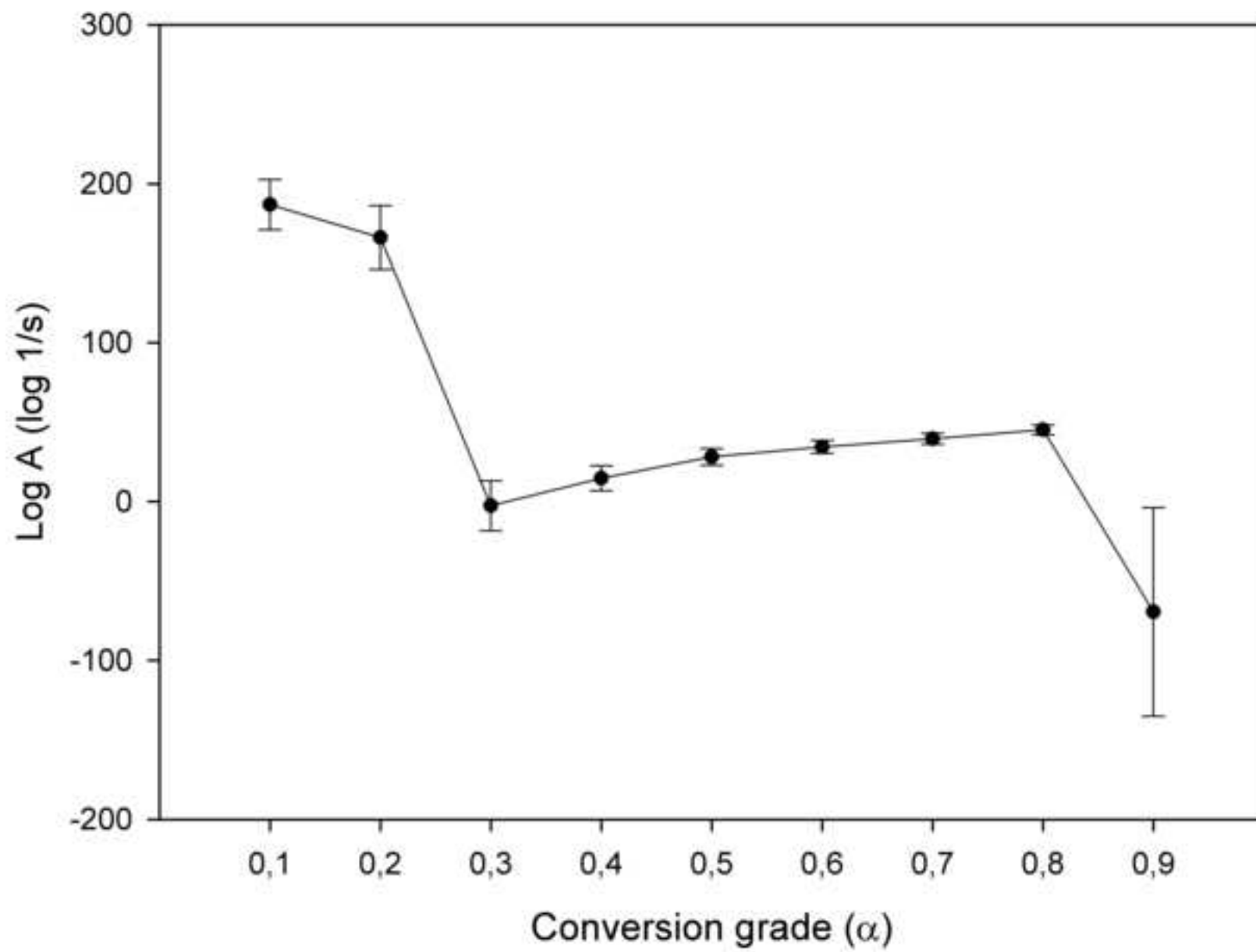


Table 1. Statistical parameters for pyrite oxidative thermochemical behavior under several kinetic methods.

1

Kinetic Method	R <sup>2</sup>	Sum of dev. squares	Mean residuals	Student coef. 95%
ASTME1641-16	0.851	136415.21	9.45	1.9
Friedman	0.913	108294.27	7.26	1.9
Ozawa-Flynn-Wall	0.969	85452.26	6.07	1.9
KAS	0.992	564.13	1.09	1.9

2